Arch. Pharm. Res. (2017) 40:480–491
DOI 10.1007/s12272-017-0904-3

Online ISSN 1976-3786
Print ISSN 0253-6269

Archives of Pharmacal Research
www.springer.com/12272

RESEARCH ARTICLE

Evaluation of the inhibitory effects of eckol and dieckol isolated from edible brown alga *Eisenia bicyclis* on human monoamine oxidases A and B

Hyun Ah Jung[1] · Anupom Roy[2] · Jee H. Jung[3] · Jae Sue Choi[2]

Received: 7 July 2016 / Accepted: 21 February 2017 / Published online: 1 March 2017

Abstract Eckol and dieckol are important phlorotannins found in edible brown algae including *Eisenia bicyclis, Ecklonia stolonifera,* and others. Inhibition of monoamine oxidase (MAO) play an important role in the early management of Parkinson's disease (PD). The aim of this study was to determine the effectiveness of eckol and dieckol isolated from the methanolic extract of *E. bicyclis* against PD by the inhibition of *human* MAO-A and MAO-B (*h*MAO-A and *h*MAO-B). A sensitive enzyme-based chemiluminescent assay and kinetics methods were used to investigate enzyme inhibition and mode of inhibition. A molecular docking simulation was performed to clarify the binding characteristics of eckol and dieckol to *h*MAO-A and *h*MAO-B. The results suggested that methanolic extract of *E. bicyclis* and its isolated phlorotannins, eckol and dieckol, have potent inhibitory activity against *h*MAO-A and *h*MAO-B. The enzyme-based kinetics results demonstrated eckol mixed and non-competitive inhibition of *h*MAO-A and *h*MAO-B, respectively, while dieckol non-competitively inhibited both *h*MAOs. Molecular docking simulation predicted that eckol and dieckol exhibit higher binding affinity towards *h*MAO-A and *h*MAO-B through hydrogen bonding and hydrophobic interactions. These findings implicate eckol and dieckol as inhibitors of *h*MAOs that might be of potential value in the management of PD.

Keywords *Eisenia bicyclis* · MAO inhibitor · Eckol · Dieckol · Molecular docking · Enzyme kinetic

Introduction

Parkinson's disease (PD) is an exceedingly prevalent neurodegenerative disorder in the aging population, particularly in developed countries (Abdullah et al. 2015), second only to Alzheimer's disease. The basis of PD appears to be the reduction of the dopamine level in neuronal synapses. Therefore, dopaminergic agonists are thought to play a crucial role in the therapy of PD.

Monoamine oxidases (MAOs) inhibitors also are important in the treatment of PD. MAOs are flavoproteins that catalyze the oxidative deamination of a mixture of neurotransmitters, such as norepinephrine, dopamine, and serotonin, as well as different exogenous and endogenous amines (i.e., tyramine, benzylamine, etc.) to their corresponding aldehydes (Lin et al. 2003). MAO exists as two isoforms, MAO-A and MAO-B, which are encoded by distinct genes sharing 70% sequence identity and the dependence on the covalently linked flavin adenine dinucleotide (FAD) cofactor in their amino acid active sites (Bach et al. 1988). The active sites of MAOs can accommodate different substrates and can be targeted by specific inhibitors. Several studies have implicated inhibitors of MAO A and B in the attenuation of oxidative stress (Sturza et al. 2013; Friedman et al. 2011). Generally, MAO-A inhibitors are used as antidepressant agents in treatment of depressive illness featuring a deficiency of serotonin and,

Hyun Ah Jung and Anupom Roys have contributed equally to this work.

✉ Jae Sue Choi
choijs@pknu.ac.kr

[1] Department of Food Science and Human Nutrition, Chonbuk National University, Jeonju 561-756, Republic of Korea

[2] Department of Food and Life Science, Pukyong National University, Busan 608-737, Republic of Korea

[3] College of Pharmacy, Pusan National University, Busan 609-735, Republic of Korea

to a lesser extent, norepinephrine (Lum and Stahl 2012; Schwartz 2013). MAO-B inhibitors are used in the therapy of PD where the key deficiency of dopamine is responsible for the characteristic motor deficits (Fernandez and Chen 2007). MAO-B is more abundant and more dynamic in the human basal ganglia (Youdim and Riederer 2007).

Monoamine oxidase inhibitors (MAOIs) have been widely employed clinically, but the use of nonselective and selective MAO-A inhibitors decreased after the recognition that these drugs potentiate the sympathomimetic effects of the dietary amine, tyramine (Da Prada et al. 1988; Flockhart 2012). Due to this interaction, blood pressure increases abnormally (the "cheese effect"). Selective MAO-B inhibitors do not cause tyramine-induced high blood pressure and the development of reversible MAO-A inhibitors that have low risk of the cheese effect have facilitated the continued role of MAOIs in the clinic (Finberg 2014). The older, irreversible MAO-A inhibitors are still used to treat certain types of depression. But from a drug design and drug safety point of view, reversible inhibition of MAO-A is a more desirable property; such drugs would not require dietary restrictions (Bonnet 2003; Provost et al. 1992). Both reversible and irreversible MAO-B inhibitors have excellent safety profiles and are not associated with changes in blood pressure (Finberg and Gillman 2011; Pae et al. 2012). The discovery of novel classes of compounds with potent inhibition activity is of interest.

Eisenia bicyclis (Kjellman) Setchell is a perennial brown alga (Phaeophyta), which belongs to the Laminariaceae family and is distributed along the mid-Pacific coastlines of Korea and Japan. It is consumed as a raw material for sodium alginate and phlorotannin-rich raw materials (Okada et al. 2004). Phlorotannins are secondary metabolites of phloroglucinol (1,3,5-trihydroxybenzene) that polymerize through ether, phenyl, or 1,4-dibenzodioxin linkages (Okada et al. 2004). Eckol and dieckol are well-known phlorotannins isolated from *E. bicyclis* (Jung et al. 2013). These phlorotannin compounds have a variety of biological activities including relief of anti-diabetic complications (Okada et al. 2004; Jung et al. 2008), antitumor (Noda et al. 1989), hepatoprotection (Kim et al. 2005), plasmin inhibition (Fukuyama et al. 1989), algicidal (Nagayama et al. 2003), tyrosinase inhibition (Kang et al. 2004), anti-inflammatory (Ryu et al. 2009), slowing of skin aging (Joe et al. 2006), anti-oxidant (Li et al. 2009), cholinesterase inhibition (Myung et al. 2005), anti-Alzheimer (Jung et al. 2010), anti-hyperlipidemic (Yoon et al. 2008), anti-diabetic (Lee et al. 2010, anti-allergic (Sugiura et al. 2006), and angiotensin converting enzyme-I inhibition (Jung et al. 2006) activities.

MAO inhibitory activity by eckol and dieckol has not been reported. This study examined the MAOs inhibitory activity of eckol, dieckol and methanol (MeOH) extract from *E. bicyclis* through an in vitro enzyme assay and molecular docking simulation.

Materials and methods

Chemicals

*h*MAO-A and *h*MAO-B were derived separately from BTI-TN-5B14 insect cells infected with recombinant baculovirus cDNA. The *h*MAO isozymes were purchased from Sigma-Aldrich (St. Louis, MO, USA) and a final concentration of 10 μg/mL of each isozyme was used. DEP (selegiline-irreversible MAO-BI) was purchased from Sigma-Aldrich.

Plant material

The leafy thalli of *E. bicyclis* were purchased from a local telemarketing company (www.ulleumgdomall.com) in Gangwon Province, Korea, in April 2014. The alga was authenticated by J. S. Choi of Pukyong National University. Voucher specimens (no. 20140428) have been deposited in the author's laboratory (J. S. Choi).

Preparation of MeOH extract of *E. bicyclis* and its major phlorotannins, eckol and dieckol

Lyophilized powder (100 g) of *E. bicyclis* leafy thallus was refluxed with MeOH (3 × 1 L) for 3 h and each filtrate was concentrated to dryness *in vacuo* at 40 °C to render the MeOH extract (34.0 g). This extract was suspended in distilled H_2O and then successively partitioned with *n*-hexane, chloroform (CH_2Cl_2), ethanol acetate (EtOAc), and butanol (*n*-BuOH) to yield the respective fractions (2.6, 2.4, 10.9, and 7.8 g), as well as H_2O residue (11.1 g). Eckol and dieckol were isolated from the EtOAc fraction as previously described (Jung et al. 2013), and identified by direct comparison with authentic samples (^{1}H and ^{13}C–NMR). The structures of eckol and dieckol are shown in Fig. 1.

*h*MAO-A and *h*MAO-B activity assay

A chemiluminescent assay was used to confirm MAO-A and MAO-B inhibitory effects of eckol, dieckol, and the MeOH extract of *E. bicyclis* using a MAO-Glo kit (Promega, Madison, WI, USA). Arbitrary light units (ALU) of the enzymes were measured in the presence of eckol, dieckol, MeOH extract, and deprenyl (DEP) as a positive control. Briefly, the *h*MAO-A and *h*MAO-B isozymes were diluted to 2× with reaction buffer (pH 7.4) and preincubated with 4× eckol, dieckol, MeOH extract, or DEP

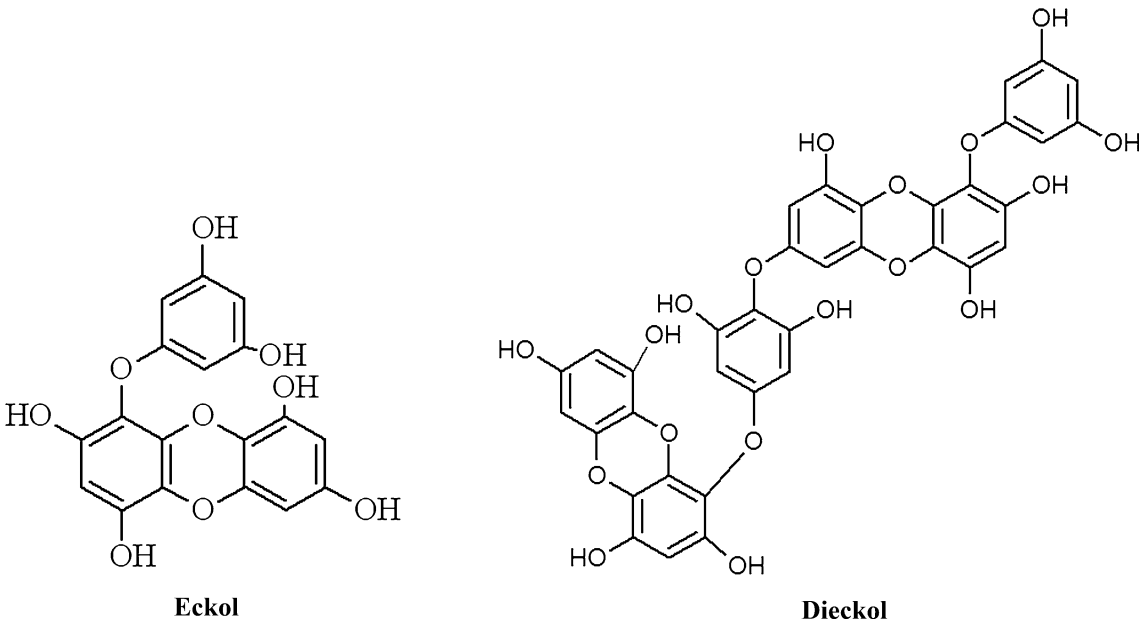

Fig. 1 Structures of eckol and dieckol

working solutions at room temperature for 1 h in white opaque 96-well plates. Final concentrations (all 5 μg/mL) of eckol, dieckol, and MeOH extract, and 2 μg/mL were used to determine MAO-B inhibition activity. Eckol, dieckol, MeOH extract (4×), and DEP working solutions were serially diluted in reaction buffer (pH 7.4) to determine the IC_{50}. The sample was substituted with reaction buffer for controls, and only reaction buffer was used as the blank. Based on our preliminary optimizations and as previously described (Valley et al. 2006), the reaction was initiated by adding 4× luciferin derivative substrate (LDS) to produce a final concentration of 40 and 4 μM for the *h*MAO-A and *h*MAO-B reactions, respectively. The final volume per well of each reaction was 50 μL. Reconstituted luciferin detection reagent (RLDR, 50 μL) was added to all wells and incubated for 20 min to stop the reaction and produce the luminescence signal. The ALU produced were detected using a SpectraMax Multi-Mode Reader (Molecular Devices, Sunnyvale, CA, USA).

Enzyme kinetics

Michaelis–Menten hyperbolic regression curves and parameters (K_m and V_{max}) were determined using the MAO-Glo assay after determining the best incubation time for initial velocity of activity. The assay was carried out under the same conditions in white opaque 96-well plates. Seven LDS data points differing logarithmically were acquired by preparing a serial dilution of triplicate concentrations. The substrate preparation was carried out at gradual 4× final LDS 40, 20, and 10 μM and no substrate for *h*MAO-A, and 4, 2, and 1 μM and no substrate for *h*MAO-B. Sample concentrations of 10, 50, and 100 μM were prepared in triplicate for *h*MAO-A and *h*MAO-B. Controls without samples were prepared simultaneously. A 2× enzyme concentration for a constant final concentration of 20 μg/μL was used for a 20 min incubation. The reactions were started by mixing the enzyme and inhibitor (or buffer) with 4× LDS in the wells. After a 1 h (for both *h*MAO-A and *h*MAO-B) incubation at room temperature, the initial reaction rate was inhibited by doubling the volume of each well with RLDR. The reactions were measured after 20 min with a SpectraMax Multi-Mode illuminometer (Molecular Devices). The Michaelis–Menten equation data were plotted as a nonlinear curve, which was transformed and presented as a linear curve in double reciprocal Lineweaver–Burk plots. K_m and V_{max} values were computed and presented as relative fold of change after the Michaelis–Menten equation analysis using GraphPad Prism 6.01 (GraphPad Prism Software, Inc., La Jolla, CA, USA). The dissociation constant of each isozyme-inhibitor complex (K_i) was also calculated as a global share value for each group of data, according to the competitive mode of the inhibition equation for the samples model with *h*MAO-A and *h*MAO-B.

Molecular docking simulation

Docking studies were performed with eckol and dieckol to examine qualified binding poses against MAO-A and MAO-B. The crystalline structure of *h*MAO-A with harmin (HRM, PDB ID:2z5x) and *h*MAO-B (PDB ID:1gos) with N-[(*E*)-

methyl](phenyl)-N-[(*E*)-2-propenylidene]methanaminium (NYP) were obtained from the RCSB Protein Data Bank with resolutions of 2.2 and 1.6 Å, respectively. HRM and NYP heteroatom were removed for the docking simulations, the protein was regarded as ligand free, and water molecules were removed from the protein structure using Accelrys Discovery Studio 4.1 (DS 4.1) (DS, http://www.accelrys.com; Accelrys, Inc. San Diego, CA, USA). All hydrogen atoms were added into the protein using the automated docking tool AutoDock 4.2.6 (Goodsell et al. 1996; Jones et al. 1997; Rarey et al. 1996). The HRM and NYP binding areas of the protein were considered the most likely regions for docking simulation to obtain the best ligand binding results. The three-dimensional structure data file (sdf) structure of eckol and dieckol were obtained from PubChem (CID: 145937 and CID: 3008868, respectively) and converted into pdb format using DS 4.1. The automated docking simulation was performed using Autodock tools (ADT) to assess the appropriate binding orientations and conformations of the ligand molecule with the protein inhibitor. A Lamarkian genetic algorithm method implemented in the Autodock 4.2 program was employed. Gasteiger charges were added by default, the rotatable bonds were set by the Autodock tools, and all torsions were allowed to rotate for the docking calculations. Grid maps were generated by the Autogrid program where a grid box size of 126 × 126 × 126 points with a default spacing of 0.375 Å between the grid points was used to cover almost the entire favorable protein binding site. The X, Y, and Z centers were 30.868, 28.77, and −14.856 for MAO-A (2z5x) and 53.502, 147,805, and 24.371 for MAO-B (1gos), respectively. The docking protocol for rigid and flexible ligand docking consisted of 10 independent genetic algorithms (GA) and other parameters used the ADT. Binding aspects of the MAO-A and MAO-B residues and their corresponding binding affinity scores were regarded as the best molecular interaction. The results were visualized and analyzed using UCSF Chimera (http://www.cgl.ucsf.edu/chimera/) and Ligplot.

Statistical analyses

Data analyses were performed using GraphPad Prism 6.01 software. Data are presented as mean ± standard error (SE) with triplicate replications, representing at least two independent experiments. Inhibitory potency was expressed as mean ± SE of at least two independent experiments. The IC_{50} was obtained by interpolating the best fit logarithmic concentration-inhibition curves for R^2. The selective index was determined by the ratio of IC_{50} of *h*MAO-A/IC_{50} of *h*MAO-B and K_i of *h*MAO-A/K_i of *h*MAO-B. One-way analysis of variance was used to detect differences. A p value < 0.05 was considered significant.

Results

Effect of *E. bicyclis* MeOH extract, eckol, and dieckol on *h*MAO-A and *h*MAO-B

The inhibitory effect of the MeOH extract, eckol and dieckol obtained from *E. bicyclis* as well as standard DEP were measured by a luminescence assay. The inhibitory potency of all on the MAO-A and -B isozymes was compared with that of DEP (Table 1). As demonstrated in Table 1 and Fig. 2, all displayed good inhibitory activity on both *h*MAO-A and *h*MAO-B, with more effectiveness inhibiting *h*MAO-A. The MeOH extract exerted good inhibitory activities with IC_{50} values of 16.82 ± 0.70 and 38.38 ± 1.78 μM, respectively, on *h*MAO-A and *h*MAO-B in dose-dependent manners. The luminescence assay revealed a DEP IC_{50} value for *h*MAO-A and *h*MAO-B of 10.54 ± 1.25 and 0.128 ± 0.01 μM, respectively (Table 1). Eckol significantly inhibited *h*MAO-A and *h*MAO-B, with IC_{50} values of 7.20 ± 0.71 and 83.44 ± 1.48 μM, respectively. Dieckol also showed good *h*MAO-A and *h*MAO-B inhibitory activities, with IC_{50} of 11.43 ± 1.06 and 43.42 ± 0.73 μM, respectively (Table 1).

Inhibition mode of *h*MAO-A and *h*MAO-B by eckol and dieckol

Incubation time was optimized to 1 h to inhibit *h*MAO-A and *h*MAO-B activities. The incubation period was within the range of initial velocities at the recommended substrate concentrations. The Michaelis–Menten kinetics curves of the MAOs with and without eckol/or dieckol at an initial rate of velocity (V) versus the change in luciferin derivative substrate (LDS) concentration are illustrated in Lineweaver–Burk plots (Figs. 3a, b, 4a, b). In the case of *h*MAO-A inhibition mode for eckol, all regression lines crossed in different point (V_{max}) on the y-axis, whereas the regression lines crossed at one points on the x-axis

Table 1 Inhibitory activities of MeOH extract, eckol, and dieckol from *Eisenia bicyclis*, and deprenyl on monoamine oxidase (MAO)-A and MAO-B with selective index (SI)

Compound	IC_{50} values (μM)[a]		SI[b]
	MAO-A	MAO-B	
Eckol	7.20 ± 0.71	83.44 ± 1.48	0.09
Dieckol	11.43 ± 1.06	43.42 ± 0.73	0.26
MeOH extra.	16.82 ± 0.70	38.38 ± 1.78	0.44
Deprenyl	10.54 ± 1.25	0.128 ± 0.01	82.34

[a] IC_{50} 50% Inhibition concentrations are expressed as the mean ± standard error of triplicate determinations

[b] *SI* selective index (MAO-A/MAO-B)

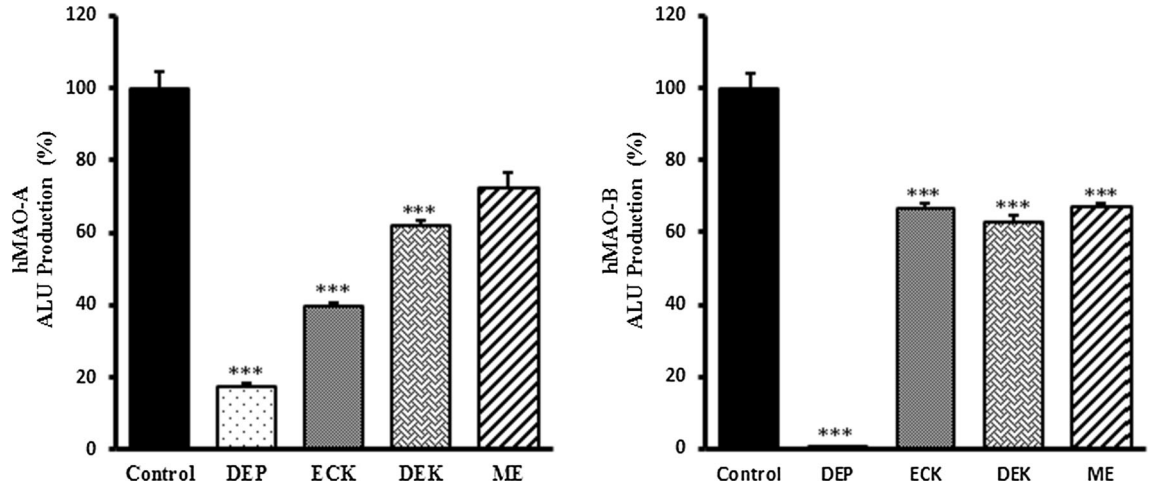

Fig. 2 Eckol (ECK) and dieckol (DEK) inhibitory efficacy on recombinant *human* monoamine oxidases (*h*MAOs) compared to *Eisenia bicyclis* methanolic extract (ME) and standard MAO inhibitor selegiline (DEP) at 5 μg/ml for MAO-A and 20 μg/ml for MAO-B (2 μg/ml for MAO-B DEP). Data are mean ± standard error of at least three determinations. ***$P < 0.05$

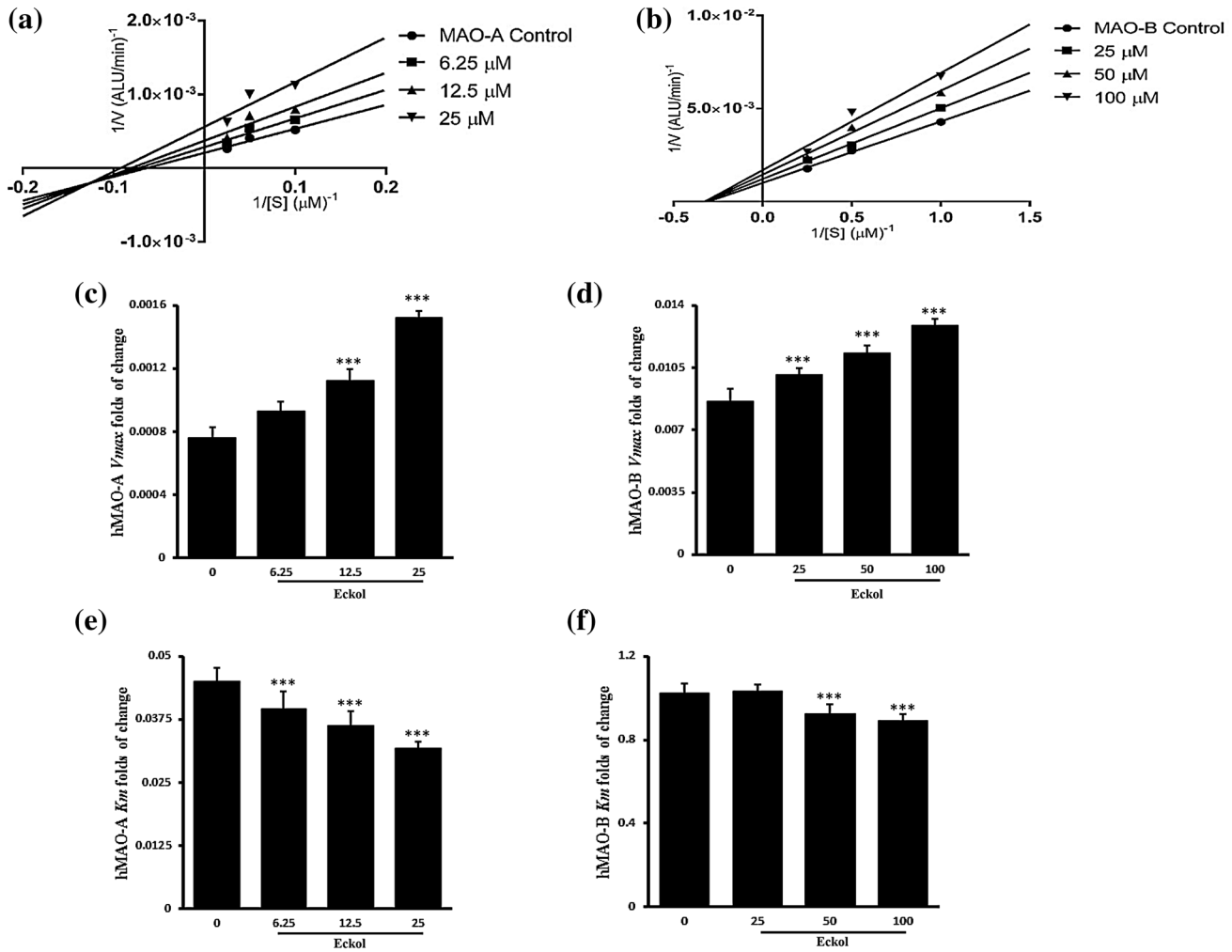

Fig. 3 Effects of eckol on *human* monoamine oxidases A and B (*h*MAO-A and *h*MAO-B) kinetics. Initial velocity (*V*) with substrate concentrations ([S]) with or without eckol as Lineweaver–Burk plots of *h*MAO-A (**a**) *h*MAO-*B* (**b**). Michaelis–Menten kinetic parameters are presented as fold-change of eckol. Parameters are maximum velocity (*Vmax*) and the Michaelis constant (*Km*) for *h*MAO-A (**c**, **e**) and *h*MAO-B (**d**, **f**), respectively. Data are mean ± standard error, n = 3, from three separate eckol experiments. ***$P < 0.05$

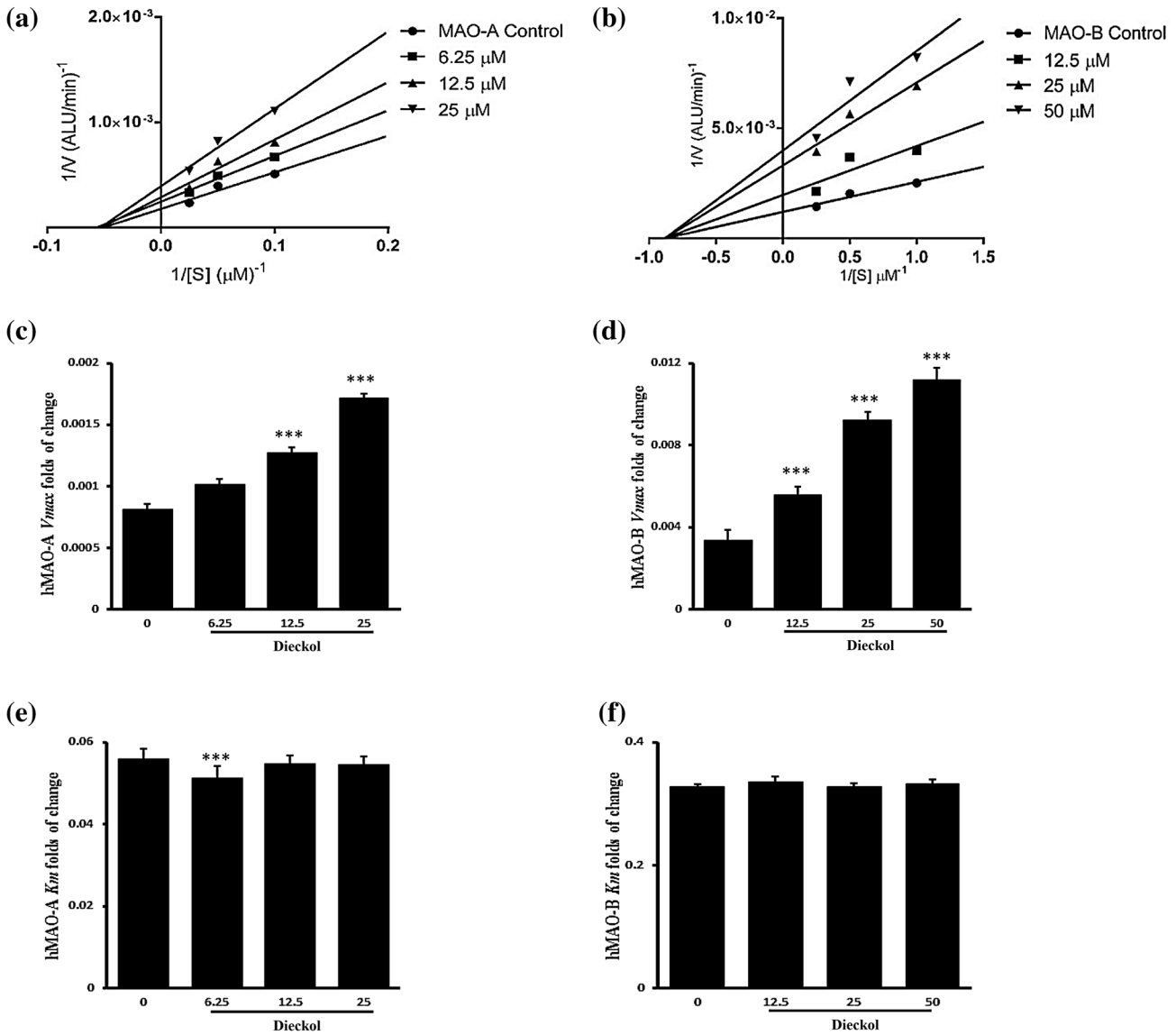

Fig. 4 Effects of dieckol on *human* monoamine oxidases A and B (*h*MAO-A and *h*MAO-B) kinetics. Initial velocity (*V*) with substrate concentrations ([S]) with or without dieckol as Lineweaver–Burk plots of *h*MAO-A (**a**) *h*MAO-*B* (**b**). Michaelis–Menten kinetic parameters are presented as fold change of dieckol. Parameters are maximum velocity (*Vmax*) and the Michaelis constant (*Km*) for *h*MAO-A (**c**, **e**) and *h*MAO-B (**d**, **f**), respectively. Data are mean ± standard error, n = 3, from three separate dieckol experiments. ***$P < 0.05$

revealing the various K_m values. These regression lines meet in one point outside of x-axes (Figs. 3a, b). All eckol regression lines crossed at different points (V_{max}) in y-axes, while that regression lines crossed at one point on the x-axis at variable K_m values towards the *h*MAO-B inhibition. Figure 3c, d depict the maximum velocity (V_{max}) with folds of change for eckol. Figure 3e, f depict the K_m values for eckol in the inhibition of *h*MAO-A and *h*MAO-B. In the case of *h*MAO-A and *h*MAO-B inhibition mode for dieckol, all regression lines crossed at different point (V_{max}) on the y-axes, while the regression lines crossed at one point on the x-axes at variable K_m values. Figure 4c, d depict the maximum velocity (V_{max}) with the fold-changes for dieckol. Likewise, Fig. 4e, f depict K_m values for dieckol for the inhibition of *h*MAO-A and *h*MAO-B.

*h*MAO-A (Figs. 5a, 6a) and *h*MAO-B (Figs. 5b, 6b) Michaelis–Menten curve with eckol and dieckol had the best fit to the mixed and non-competitive mode of inhibition using GraphPad Prism 6.01. Since K_i determination is independent of substrate, K_i was determined and calculated according to the mixed and non-competitive mode of inhibition. As shown in Table 2, K_i values of eckol were 20.26 ± 2.95 and 162.8 ± 3.45 μM for the inhibition of *h*MAO-A and *h*MAO-B, respectively. K_i values of dieckol

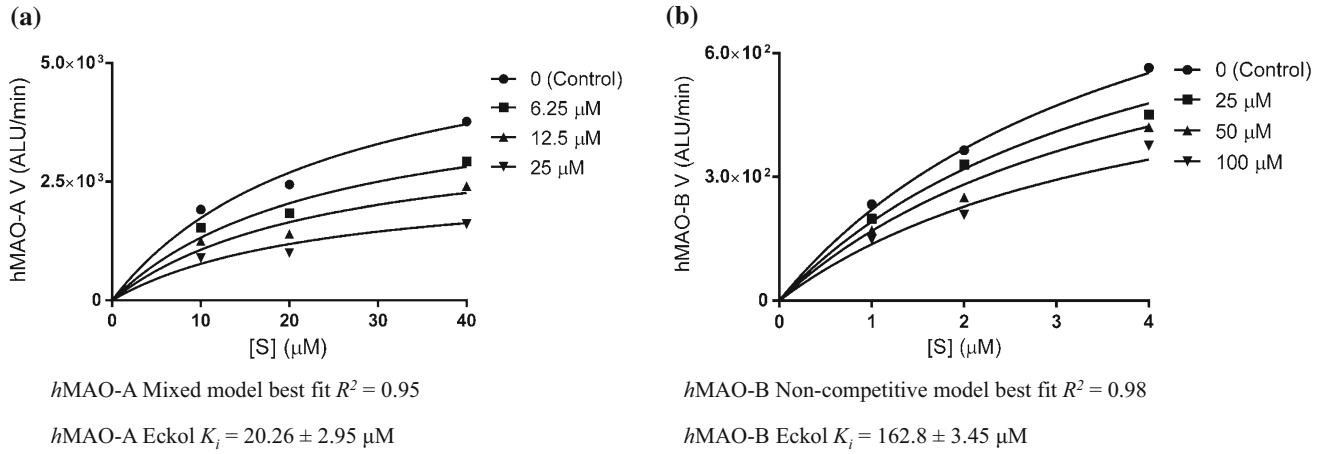

*h*MAO-A Mixed model best fit $R^2 = 0.95$

*h*MAO-A Eckol $K_i = 20.26 \pm 2.95$ μM

*h*MAO-B Non-competitive model best fit $R^2 = 0.98$

*h*MAO-B Eckol $K_i = 162.8 \pm 3.45$ μM

Fig. 5 Inhibition of *human* monoamine oxidases A (*h*MAO-A) (**a**) and B (*h*MAO-B) (**b**) by eckol best fit mixed inhibition mode for *h*MAO-A and best fit non-competitive inhibition mode for *h*MAO-B. Global share fit values of $K_i \pm$ standard error, n = 3, were calculated by GraphPad Prism 6. K_i values were calculated using the mixed for MAO-A and non-competitive for MAO-B mode of inhibition

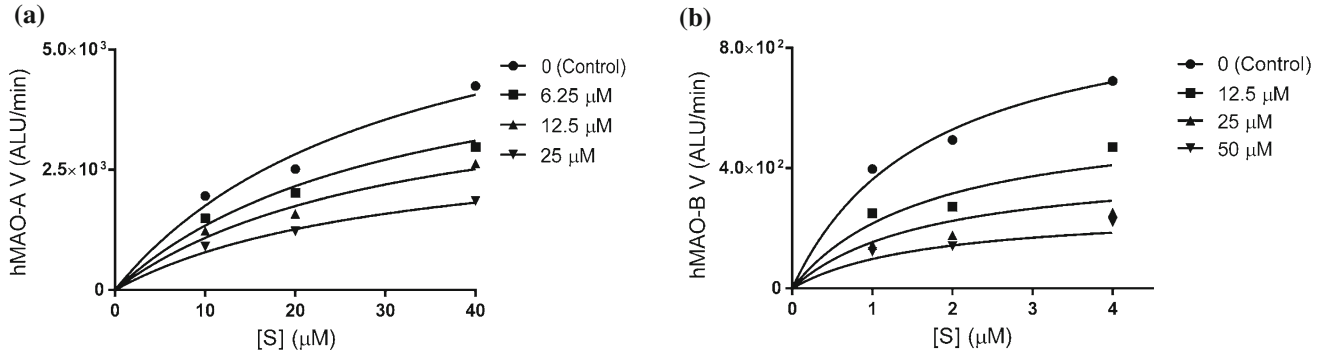

*h*MAO-A Non-competitive model best fit $R^2 = 0.97$

*h*MAO-A Dieckol $K_i = 20.28 \pm 1.08$ μM

*h*MAO-B Non-competitive model best fit $R^2 = 0.96$

*h*MAO-B Dieckol $K_i = 18.50 \pm 1.63$ μM

Fig. 6 Inhibition of *human* monoamine oxidases A (*h*MAO-A) (**a**) and B (*h*MAO-B) (**b**) by dieckol best fit the non-competitive inhibition mode. Global share fit values of $K_i \pm$ standard error, n = 3, were calculated by GraphPad Prism 6. All K_i values were calculated using the non-competitive mode of inhibition

Table 2 *Ki* value of eckol and dieckol on monoamine oxidase (MAO)-A and MAO-B with the selective index (SI) and inhibition type

Compound	*Ki* value (μM)[a]		SI[c]	Inhibition Type[b]	
	MAO-A	MAO-B		MAO-A	MAO-B
Eckol	20.26 ± 2.95	162.8 ± 3.45	0.13	Mixed	Non-competitive
Dieckol	20.28 ± 1.08	18.50 ± 1.63	1.10	Non-competitive	Non-competitive

[a,b] *Ki* value and inhibition type were determined using Graph Pad Prism 6

[c] *SI* selective index (MAO-A/MAO-B)

were 20.28 ± 1.08 and 18.50 ± 1.63 μM for the inhibition of *h*MAO-A and *h*MAO-B, respectively.

Docking analysis of eckol and dieckol into *h*MAO-A and *h*MAO-B active sites

The docking scores and orientation of eckol and dieckol at the active sites of the *h*MAO-A and *h*MAO-B crystal structures are shown in Tables 3 and 4, and Figs. 7 and 8, respectively. The crystallographic poses are visualized for both analogs in the active site of each isozyme compared to their cognate ligands (2z5x and 2v5z) and the cofactor FAD (Figs. 7a, 8a). The hydrogen bond distance, amino acid interactions, binding energy, and orientation of the docked compound within the active site are the basic criteria for successful docking of eckol and dieckol and

Table 3 Docking affinity scores and possible H-bond formation to *human* monoamine oxidase A (*h*MAO-A) (2z5x) active sites by eckol and dieckol compared with that of the inhibitor harmine (HRM)

Compounds	Autodock 4.2 score (Kcal/mol)	No. of H-bonds	H-bonds interacting residues	Van der Waals interacting residues
Harmine (HRM)	−6.95	–	–	Tyr407, Tyr444, Asn181, Gln215, Phe352, Ile180, Ile335, Leu337, Phe208
Eckol	−9.40	4	Met445, Tyr69, Gln215	Gly443, Gly67, Tyr444, Ile180, Phe352, Tyr407, Cys406, Arg51
Dieckol	−7.48	8	Tyr402, Val244, His282, Leu287, Phe283, Ile281	Leu259, Gln296, Asn292, Glu286, Ala279, Lys280, Pro243

Table 4 Docking affinity scores and possible H-bond formation to *human* monoamine oxidase B (*h*MAO-B) (1gos) active sites by eckol and dieckol compared with that of the inhibitor N-[(*E*)-methyl](phenyl)-N-[(*E*)-2-propenylidene]methanaminium (NYP)

Compounds	Autodock 4.2 Score (Kcal/mol)	No. of H-bonds	H-bonds interacting residues	Van der Waals interacting residues
Harmine (HRM)	−6.95	–	–	Tyr407, Tyr444, Asn181, Gln215, Phe352, Ile180, Ile335, Leu337, Phe208
Eckol	−9.40	4	Met445, Tyr69, Gln215	Gly443, Gly67, Tyr444, Ile180, Phe352, Tyr407, Cys406, Arg51
Dieckol	−7.48	8	Tyr402, Val244, His282, Leu287, Phe283, Ile281	Leu259, Gln296, Asn292, Glu286, Ala279, Lys280, Pro243

*h*MAOs (2z5x and 2v5z) to analyze the receptor-ligand complex model. Eckol showed lowest binding energy (−9.40 kcal/mol) with highest binding affinity as compared with reported inhibitor HRM (−6.95 kcal/mol) and dieckol (−7.48 kcal/mol) toward the inhibition of *h*MAO-A (Table 3). Eckol showed four hydrogen bond interactions with *h*MAO-A active site residues (Met445, Tyr69, and Gln215) (Fig. 7c). Some hydrophobic interactions were also observed between Gly443, Gly67, Tyr444, Ile180, Phe352, Tyr407, Cys406, and Arg51 with eckol towards *h*MAO-A inhibition. Dieckol also showed good binding affinity (−7.48 kcal/mol) in *h*MAO-A inhibition by forming eight hydrogen bond interactions. Dieckol displayed hydrophobic interaction with Leu259, Gln296, Asn292, Glu286, Ala279, Lys280, and Pro243 residues of the *h*MAO-A active site.

Dieckol exhibited lowest binding energy (−7.89 kcal/mol) with a highest binding affinity in *h*MAO-B inhibition compared to the reported inhibitor NYP (−5.65 kcal/mol) and eckol (−6.77 kcal/mol). Dieckol had eight hydrogen bond interactions in the inhibition of *h*MAO-B (Table 4). Along with hydrogen bonds, dieckol also showed several hydrophobic interactions with the active site residues of *h*MAO-B (Fig. 8). In the case of *h*MAO-B inhibition, eckol showed good inhibitory potency with binding energy (−6.77 kcal/mol). Trp119, His115, Val106, Asn116, and Arg120 residues were involved with eckol in hydrogen bond interactions. Likewise, Asp123, Phe103, Glu483, Pro104, and Tyr112 residues interacted with eckol in hydrophobic interactions (Fig. 8).

Discussion

Brown algae are sea vegetables that are a popular food and health food in China, Japan, and South Korea (Nisizawa et al. 1987). The biological and pharmacological activities of marine brown algae have been clarified, which has revealed brown algae to be an enriched source of highly bioactive secondary metabolites that may be exploited in the development of novel pharmaceutical agents (Ali 2010). Biologically active compounds identified from brown algae include phlorotannins, diterpenes, polysaccharides, phytosterols, and phytopigments.

Of these compounds, phlorotannins—especially eckol and dieckol—have the greatest potential as a functional ingredient in food products, pharmaceuticals, and cosmeceuticals due to bioactivities that include antioxidant, bactericidal, anti-HIV, anticancer, radioprotective, antiallergic, and inhibition of α-glucosidase, α-amylase, angiotensin-I converting enzyme, matrix metalloproteinases, hyaluronidase, and tyrosinase (Li et al. 2011), neuroprotective effect on amyloid beta peptide-induced toxicity in PC12 cells (Ahn et al. 2012), and inhibition of acetylcholinesterase, butyrylcholinesterase and BACE1 in the treatment of Alzheimer's disease (AD) (Li et al. 2011; Jung et al. 2010).

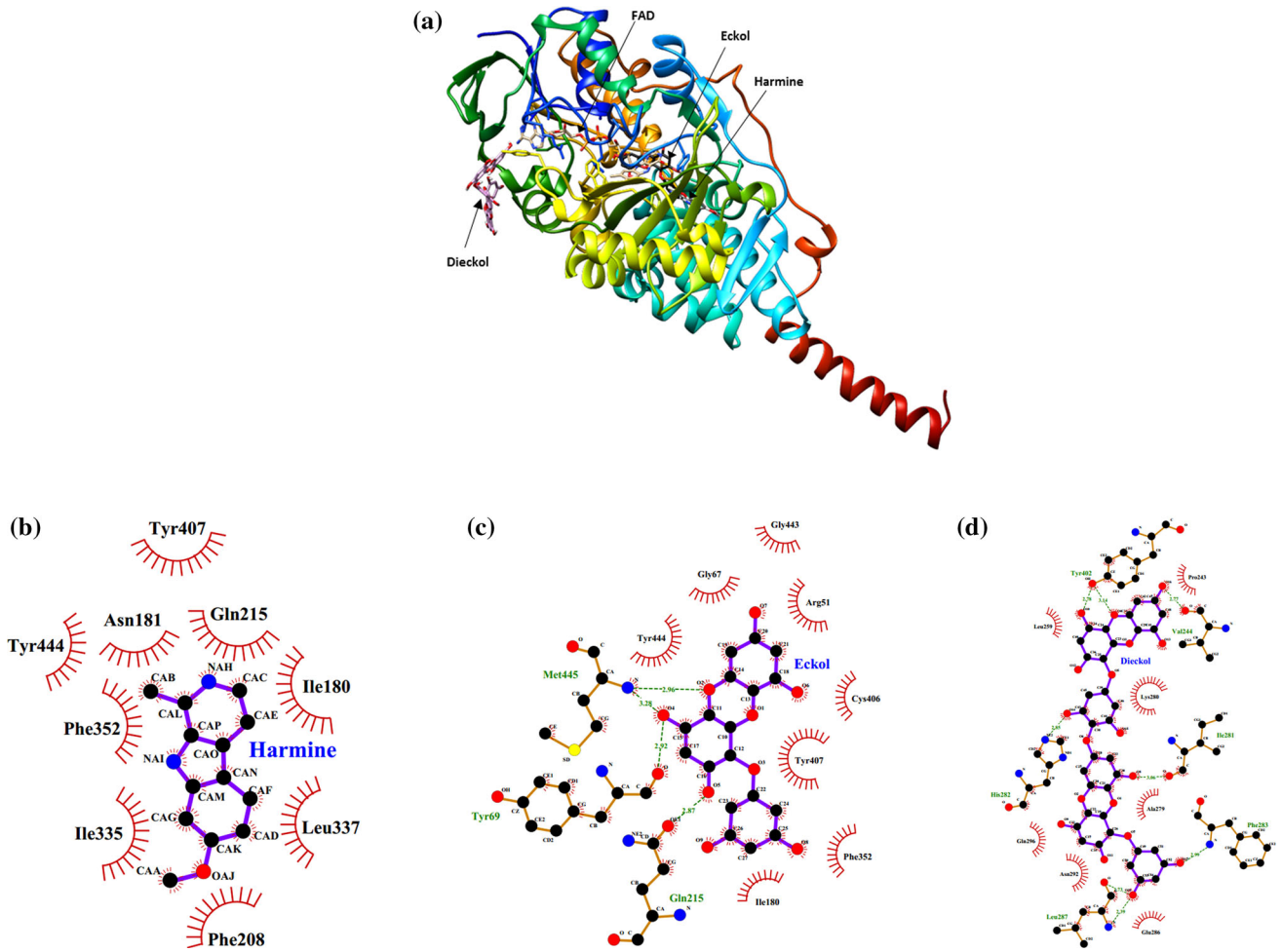

Fig. 7 Binding poses between *human* monoamine oxidase A (*h*MAO-A) and eckol, dieckol along with cofactor FAD and inhibitor harmine (HRM) (**a**). Binding mode of harmine, eckol and dieckol to the *h*MAO-A (2z5x) active sites (**b–d**)

The present study was prompted by our idea that methanol (MeOH) extract of *E. bicyclis*, and the isolated eckol and dieckol constituents might have activity against *h*MAO isozymes for the treatment of PD. An in vitro enzyme assay and molecular docking simulation were used to explore this idea.

The two-step highly sensitive functional luminescence assay was used to investigate *h*MAO inhibitory activities of the MeOH extract, eckol, and dieckol (Fig. 2). The luminescence assay was more useful than a spectrophotometric assay to determine inhibitory efficacy, potency, selectivity, and mode of inhibition of MeOH extract, eckol, and dieckol. The effects of MeOH extract, eckol, and dieckol on *h*MAO-A and *h*MAO-B activities were very clear compared to that of DEP positive control (Fig. 2). Eckol and dieckol showed potent *h*MAO-A inhibitory IC_{50} values of 7.20 ± 0.71 and 11.43 ± 1.06 μM, respectively, whereas DEP showed inhibitory IC_{50} of 10.54 ± 1.25 μM for *h*MAO-A (Table 1). MeOH extract also showed good inhibitory IC_{50} of 16.82 ± 0.70 μM for *h*MAO-A. On the other hand, both eckol and dieckol showed significant inhibitory IC_{50} values of 83.44 ± 1.48 and 43.42 ± 0.73 μM for *h*MAO-B, respectively (Table 1). Positive control DEP showed inhibitory IC_{50} of 0.128 ± 0.01 μM for *h*MAO-B (Table 1). In the case of *h*MAO-B inhibition, dieckol was more potent than eckol. Interestingly, MeOH extract exhibited higher *h*MAO-B inhibitory activity with lower IC_{50} of 38.38 ± 1.78 μM compared with the inhibitory activity of eckol and dieckol inhibitory. This means that MeOH extract contains other compounds besides eckol and dieckol. In fact, MeOH extract derived brown alga contains different kinds of phlorotannins. This is the first work demonstrating the anti-PD activity of marine edible brown algae and its phlorotannins via inhibiting MAOs.

To explore the mechanism of enzyme inhibition by eckol and dieckol, kinetic analyses were performed at different concentrations of substrate and using various concentrations of eckol and dieckol. Mixed and non-competitive inhibitions were shown by eckol and dieckol after

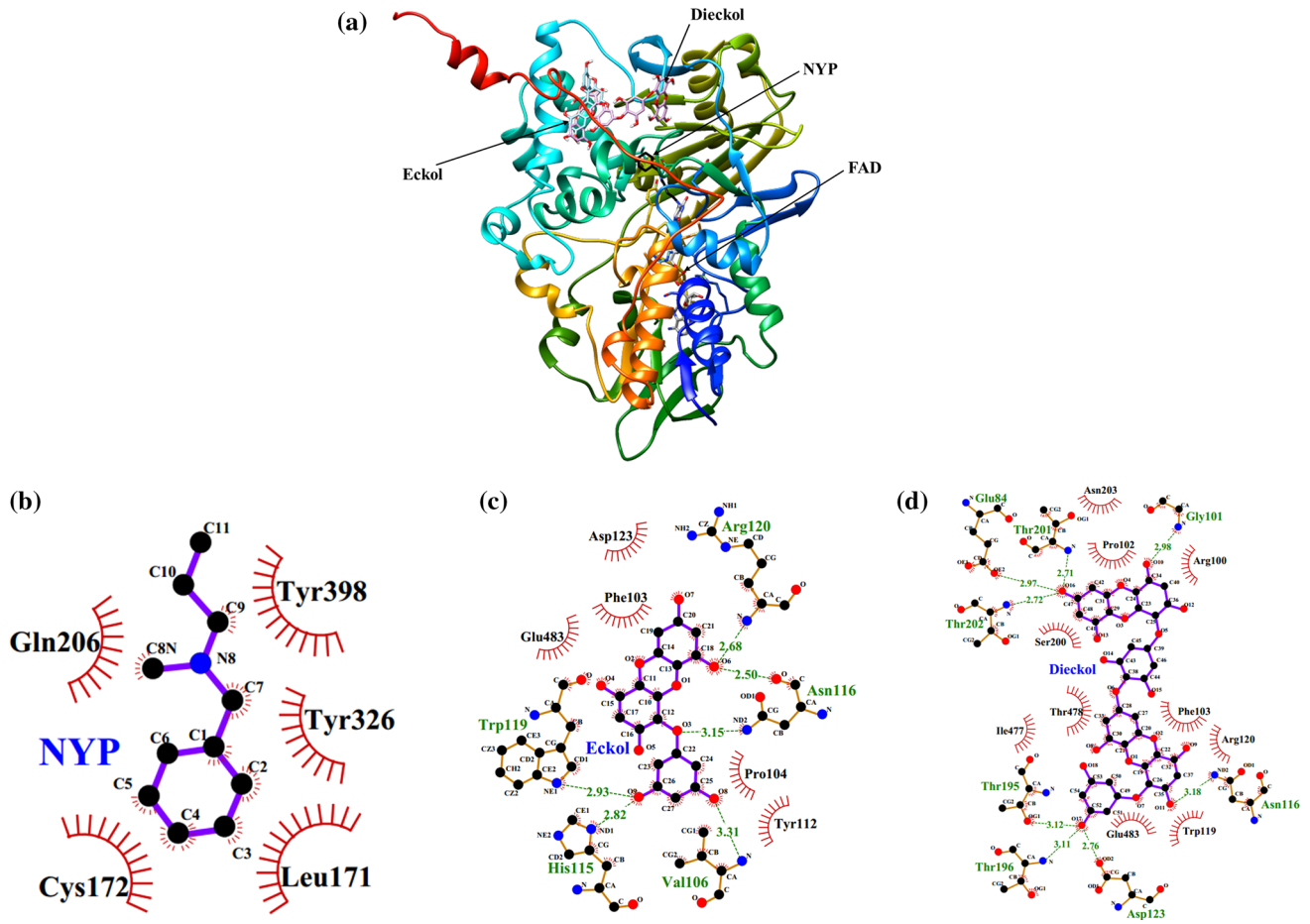

Fig. 8 Binding poses between *human* monoamine oxidase B (*h*MAO-B) and eckol, dieckol along with cofactor FAD and inhibitor N-[(*E*)-methyl](phenyl)-N-[(*E*)-2-propenylidene]methanaminium (NYP) (**a**). Binding mode of NYP, eckol, and dieckol to the *h*MAO-B (1gos) active sites (**b–d**)

preparing double-reciprocal and Lineweaver–Burk plots for *h*MAO-A and *h*MAO-B (Figs. 3, 4). Eckol showed a mixed and non-competitive mode of inhibition for *h*MAO-A and *h*MAO-B (Fig. 3), whereas dieckol showed a non-competitive mode of inhibition for both MAO isozymes (Fig. 4). Both eckol and dieckol showed reversible inhibitory activity on MAOs, which is important for the development of enzyme inhibitors. The *Ki* value for eckol to inhibit *h*MAO-A and *h*MAO-B isozymes was 20.26 ± 2.95 and 162.8 ± 3.45 µM, respectively (Fig. 5). The respective *Ki* values for dieckol were 20.28 ± 1.08 and 18.50 ± 1.63 µM. The lower K_i values of eckol and dieckol to inhibit *h*MAO-A compared to *h*MAO-B implied tighter binding of eckol and dieckol to *h*MAO-A, and presumably more effective inhibition.

We also carried out molecular docking simulations to determine the mechanism of the interactions between eckol/or dieckol, and the active site of MAOs isozymes. Molecular docking is a computational technique that has been validated as a means of exploring possible binding modes of a ligand to a given receptor, or another binding site (Goodsell et al. 1996). Eckol showed higher binding affinity with lower binding energy (−9.40 kcal/mol) to *h*MAO-A than *h*MAO-B (−6.77 kcal/mol). The NYP inhibitor showed binding affinity of −5.65 kcal/mol for *h*MAO-B and HRM had a −6.95 kcal/mol binding affinity of *h*MAO-A. The Met445, Tyr69, and Gln215 *h*MAO-A active site residues formed strong hydrogen bonds with eckol hydroxyl groups (O2, O4, and O5). The eckol-*h*MAO-A complex was further stabilized by hydrophobic interactions with the −Gly443, Gly67, Tyr444, Ile180, Phe352, Tyr407, Cys406, and Arg51 residues. On the other hand, dieckol showed higher binding affinity with lower binding energy (−7.89 kcal/mol) to *h*MAO-B than *h*MAO-A (−7.48 kcal/mol). The Gly101 and Asn116 *h*MAO-B active sites residues formed hydrogen bonds with OH groups (O10 and O11) of dieckol. Similarly, the -Thr201, Glu84, and Thr202 residues interacted with the dieckol O16 hydroxyl group through hydrogen bonds, whereas the -Thr195, Thr196, and Asp123 residues formed hydrogen

bonds with dieckol hydroxyl group (O17). The dieckol–*h*MAO-B complex was further strengthened by hydrophobic interactions with -Asn203, Pro102, Arg100, Ser200, Ile477, Thr478, Glu483, Trp119, Arg120, and Phe103 residues. Eckol exhibited lower binding energy than dieckol to inhibit *h*MAO-A isozyme, but dieckol also showed good inhibitory binding energy (−7.48 kcal/mol) compared to HRM (−6.95 kcal/mol). Likewise, eckol showed significant binding energy (−6.77 kcal/mol) towards the inhibition of *h*MAO-B isozyme compared to NYP (−5.65 kcal/mol).

The molecular docking analysis of eckol and dieckol on *h*MAO-A and *h*MAO-B crystalline structures predicted very different binding behaviors, which were illustrated in a LigPlot + analysis (Laskowski and Swindells 2011) (Figs. 7b–d, 8b–d). During this docking simulation, the presence of hydroxyl group in the compound structure was very important and increased the tendency of hydrogen bond interaction. There are more hydroxyl groups in dieckol than in eckol structure, which was reflected in the greater hydrogen bond interaction of dieckol compared to eckol in the inhibition of the MAO-A and MAO-B isozymes. No specific residues were responsible for the inhibition of the MAO-A and MAO-B isozymes. Concerning the inhibition of *h*MAO-A, the inhibitory activity of eckol differed from that of dieckol, likely reflecting their different binding sites on *h*MAO-A (Fig. 7a). Similarly, the difference in the inhibitory activity of eckol and dieckol for *h*MAO-B was reflected in the crystallographic structures (Fig. 8a).

Eckol and dieckol have not been used to treat PD, However, both possess anti-inflammatory activities (Jung et al. 2013) and a neuroprotective effect on amyloid beta peptide-induced toxicity in PC12 cells (Ahn et al. 2012). PD is related with oxidative stress (Hwang 2013). Eckol and dieckol have antioxidant activity (Kang et al. 2003; 2013). Eckol and dieckol also potently inhibit peroxisome proliferator-activated receptor γ (Jung et al. 2014), which protect against PD neurodegeneration (Carta 2013). The capability of oral absorption and the ability of both eckol and dieckol to cross the blood–brain barrier could be of potential value in the treatment of PD, if these attributes can be proven in future studies. The present in vitro data studies suggest that eckol and dieckol inhibit MAOs; in vivo studies are needed for confirmation. The anti-inflammatory properties and neuroprotective activities of eckol and dieckol in addition to their reversible inhibition of the MAO enzymes implicate them as useful compounds for PD therapy.

In conclusion, the marine phlorotannins, eckol and dieckol can reversibly inhibit MAOs. Biochemical and molecular docking examinations revealed mixed and non-competitive catalytic site related mechanisms. Hence, eckol and dieckol could be safer substitutes for currently used classical MAOs inhibitors. Eckol and dieckol could be a novel class of natural reversible MAO inhibitor. The properties of these phlorotannins may be of value to therapeutically manage PD and other neurological disorders.

Acknowledgements This research was supported by the Basic Science Research Program through the National Research Foundation of Korea (NRF), funded by the Ministry of Education (2012R1A6A1028677).

Compliance with ethical standards

Conflicts of interest The authors declare no conflicts of interest.

References

Abdullah R, Basak I, Patil KS, Alves G, Larsen JP, Moller G (2015) Parkinson's disease and age: the obvious but largely unexplored link. Exp Gerontol 68:33–38

Ahn BR, Moon HE, Kim HR, Jung HA, Choi JS (2012) Neuroprotective effect of edible brown alga *Eisenia bicyclis* on amyloid beta peptide-induced toxicity in PC12 cells. Arch Pharm Res 35:1989–1998

Ali AEG (2010) Biological importance of marine algae. Saudi Pharm J 18:1–25

Bach AW, Lan NC, Johnson DL, Abell CW, Bembenek ME, Kwan SW, Seeburg PH, Shih JC (1988) cDNA cloning of human liver monoamine oxidase A and B: molecular basis of differences in enzymatic properties. Proc Natl Acad Sci USA 85:4934–4938

Bonnet U (2003) Moclobemide: therapeutic use and clinical studies. Drug Rev 9:97–140

Carta AR (2013) PPAR-γ: therapeutic prospects in Parkinson's disease. Curr Drug Targets 14:743–751

Da Prada M, Zurcher G, Wuthrich I, Haefely WE (1988) On tyramine, food, beverages and the reversible MAO inhibitor moclobemide. J Neural Transm Suppl 26:31–56

Fernandez HH, Chen JJ (2007) Monoamine oxidase-B inhibition in the treatment of Parkinson's disease. Pharmacotherapy 27:174S–185S

Finberg JP (2014) Update on the pharmacology of selective inhibitors of MAO-A and MAO-B: focus on modulation of CNS monoamine neurotransmitter release. Pharmacol Ther 143:133–152

Finberg JP, Gillman K (2011) Selective inhibitors of monoamine oxidase type B and the "cheese effect". Int Rev Neurobiol 100:169–190

Flockhart DA (2012) Dietary restrictions and drug interactions with monoamine oxidase inhibitors: an update. J Clin Psychiatr 73:17–24

Friedman A, Arosio P, Finazzi D, Koziorowski D, Galazka-Friedman J (2011) Ferritin as an important player in neurodegeneration. Parkinsonism Relat Disord 17:423–430

Fukuyama Y, Kodama M, Miura J, Kinzyo Z, Mori H, Nakayama Y, Takahashi M (1989) Structure of an anti-plasmin inhibitor, eckol, isolated from the brown alga *Ecklonia kurome* Okamura and inhibitory activities of its derivatives on plasma plasmin inhibitors. Chem Pharm Bull 37:349–353

Goodsell DS, Morris GM, Olson AJ (1996) Automated docking of flexible ligands: applications of AutoDock. J Mol Recognit 9:1–5

Hwang O (2013) Role of oxidative stress in Parkinson's disease. Exp Neurobiol 22:11–17

Joe MJ, Kim SN, Choi HY, Shin WS, Park GM, Kang DW, Kim YK (2006) The inhibitory effects of eckol and dieckol from *Ecklonia stolonifera* on the expression of matrix metalloproteinase-I in human dermal fibroblasts. Biol Pharm Bull 29:1735–1739

Jones G, Willett P, Glen RC, Leach AR, Taylor R (1997) Development and validation of a genetic algorithm for flexible docking. J Mol Biol 267:727–748

Jung HA, Hyun SK, Kim HR, Choi JS (2006) Angiotensin-I converting enzyme inhibitory activity of phlorotannins from *Ecklonia stolonifera*. Fish Sci 72:1292–1299

Jung HA, Yoon NY, Woo MH, Choi JS (2008) Inhibitory activities of extracts from several kinds of seaweeds and phlorotannins from the brown alga *Ecklonia stolonifera* on glucose-mediated protein damage and rat lens aldose reductase. Fish Sci 74:1363–1365

Jung HA, Oh SH, Choi JS (2010) Molecular docking studies of phlorotannins from *Eisenia bicyclis* with BACE1 inhibitory activity. Bioorg Med Chem Lett 20:3211–3215

Jung HA, Jin SE, Ahn BR, Lee CM, Choi JS (2013) Anti-inflammatory activity of edible brown alga *Eisenia bicyclis* and its constituents fucosterol and phlorotannins in LPS-stimulated RAW264.7 macrophages. Food Chem Toxicol 59:199–206

Jung HA, Jung HJ, Jeong HY, Kwon HJ, Ali MY, Choi JS (2014) Phlorotannins isolated from the edible brown alga *Ecklonia stolonifera* exert anti-adipogenic activity on 3T3-L1 adipocytes by downregulating C/EBPα and PPARγ. Fitoterapia 92:260–269

Kang HS, Chung HY, Jung JH, Son BW, Choi JS (2003) A new phlorotannin from the brown alga *Ecklonia stolonifera*. Chem Pharm Bull 51:1012–1014

Kang HS, Kim HR, Byun DS, Son BW, Namg TJ, Choi JS (2004) Tyrosinase inhibitors isolated from the edible brown alga *Ecklonia stolonifera*. Arch Pharm Res 27:1226–1232

Kang MC, Cha SH, Wijesinghe WA, Kang SM, Lee SH, Kim EA, Song CB, Jeon YJ (2013) Protective effect of marine alage phlorotannins against AAPH-induced oxidative stress in zebrafish embryo. Food Chem 138:950–955

Kim YC, An RB, Yoon NY, Nam TJ, Choi JS (2005) Hepatoprotective constituents of the edible brown alga *Ecklonia stolonifera* on tacrine-induced cytotoxicity in Hep G2 cells. Arch Pharm Res 28:1376–1380

Laskowski RA, Swindells MB (2011) LigPlot+: multiple ligand-protein interaction diagrams for drug discovery. J Chem Inf Model 51:2778–2786

Lee SH, Park MH, Heo SJ, Kang SM, Ko SC, Han JS, Jeon YJ (2010) Dieckol isolated from *Ecklonia cava* inhibits a-glucosidase and a-amylase in vitro and alleviates postprandial hyperglycemia in streptozotocin-induced diabetic mice. Food Chem Toxicol 48: 2633–2637

Li Y, Qian ZJ, Ryu B, Lee SH, Kim MM, Kim SK (2009) Chemical components and its antioxidant properties in vitro: an edible marine brown alga, *Ecklonia cava*. Bioorg Med Chem 17:1963–1973

Li YX, Wijesekara I, Li Y, Kim SK (2011) Phlorotannins as bioactive agents from brown algae. Process Biochem 46:2219–2224

Lin RD, Hou WC, Yen KY, Lee MH (2003) Inhibition of monoamine oxidase B (MAO-B) by Chinese herbal medicines. Phytomedicine 10:650–656

Lum CT, Stahl SM (2012) Opportunities for reversible inhibitors of monoamine oxidase-A (RIMAs) in the treatment of depression. CNS Spectr 17:107–120

Myung CS, Shin HC, Bao HY, Yeo SJ, Lee BH, Kang JS (2005) Improvement of memory by dieckol and phlorofucofuroeckol in ethanol-treated mice: possible involvement of the inhibition of acetylcholinesterase. Arch Pharm Res 28:691–698

Nagayama K, Shibata T, Fujimoto K, Honjo H, Nakamura T (2003) Algicidal effect of phlorotannins from the brown alga *Ecklonia kurome* on red tide microalgae. Aquaculture 218:601–611

Nisizawa K, Noda H, Kikuchi R, Watanabe T (1987) The main seaweed foods in Japan. Hydrobiology 151:5–29

Noda H, Amano H, Arashima K, Hashimoto S, Nisizawa K (1989) Studies on the antitumor activity of marine algae. Nippon Suisan Gakk 55:1259–1264

Okada Y, Ishimaru A, Suzuki R, Okuyama T (2004) A new phloroglucinol derivative from the brown alga *Eisenia bicyclis*: potential for the effective treatment of diabetic complications. J Nat Prod 67:103–105

Pae CU, Bodkin JA, Portland KB, Thase ME, Patkar AA (2012) Safety of selegiline transdermal system in clinical practice: analysis of adverse events from postmarketing exposures. J Clin Psychiatr 73:661–668

Provost JC, Funck-Brentano C, Rovei V, D'Estanque J, Ego D, Jaillon P (1992) Pharmacokinetic and pharmacodynamics interaction between toloxatone, a new reversible monoamine oxidase-A inhibitor, and oral tyramine in healthy subjects. Clin Pharmacol Ther 52:384–393

Rarey M, Kramer B, Lengauer T, Klebe G (1996) A fast flexible docking method using an incremental construction algorithm. J Mol Biol 261:470–489

Ryu B, Li Y, Qian ZJ, Kim MM, Kim SK (2009) Differentiation of human osteosarcoma cells by isolated phlorotannins is subtly linked to COX-2, iNOS, MMPs, and MAPK signaling: implication for chronic articular disease. Chem Biol Interact 179:192–201

Schwartz TL (2013) A neuroscientific update on monoamine oxidase and its inhibitors. CNS Spectr 18:25–32

Sturza A, Leisegang MS, Babelova A, Schroder K, Benkhoff S, Loot AE, Fleming I, Schulz R, Muntean DM, Brandes RP (2013) Monoamine oxidases are mediators of endothelial dysfunction in the mouse aorta. Hypertension 62:140–146

Sugiura Y, Matsuda K, Yamada Y, Nishikawa M, Shioya K, Katsuzaki H, Imai K, Amano H (2006) Isolation of a new antiallergic phlorotannin, phlorofucofuroeckol-B, from an edible brown alga, *Eisenia arborea*. Biosci Biotechnol Biochem 70:2807–2811

Valley MP, Zhou W, Hawkins EM, Shultz J, Cali JJ, Worzella T, Bernad L, Good T, Good D, Riss TL, Klaubert DH, Wood KV (2006) A bioluminescent assay for monoamine oxidase activity. Anal Biochem 359:238–246

Yoon NY, Kim HR, Chung HY, Choi JS (2008) Anti-hyperlipidemic effect of an edible brown alga, *Ecklonia stolonifera*, and its constituents on poloxamer 407-induced hyperlipidemic and cholesterol-fed rats. Arch Pharm Res 31:1564–1571

Youdim MB, Riederer PF (2007) Monoamine oxidase A and B inhibitors in Parkinson's disease. Handb Clin Neurol 84:93–120